Smart Structures and Systems, *Vol. 28, No. 3 (2021) 343-354*
https://doi.org/10.12989/sss.2021.28.3.343

Static deflections and stress distribution of functionally graded sandwich plates with porosity

Lazreg Hadji*[1,2] and Abdelouahed Tounsi [3,4,5]

[1] *Laboratory of Geomatics and Sustainable Development, Ibn Khaldoun University of Tiaret, Algeria*
[2] *Department of Mechanical Engineering, University of Tiaret, BP 78 Zaaroura, Tiaret, 14000, Algeria*
[3] *Material and Hydrology Laboratory, Faculty of Technology, Civil Engineering Department, University of Sidi Bel Abbes, Algeria*
[4] *YFL (Yonsei Frontier Lab), Yonsei University, Seoul, Korea*
[5] *Department of Civil and Environmental Engineering, King Fahd University of Petroleum & Minerals, 31261 Dhahran, Eastern Province, Saudi Arabia*

(*Received September 3, 2020, Revised December 5, 2020, Accepted January 28, 2021*)

Abstract. In this paper a higher-order shear deformation plate theory is presented to investigate the stress distribution and static deflections of functionally graded sandwich plates with porosity effects. The displacement field of the present theory is chosen based on nonlinear variations in the in-plane displacements through the thickness of the plate. By dividing the transverse displacement into the bending and shear parts and making further assumptions, the number of unknowns and equations of motion of the present theory is reduced a and hence makes them simple to use. The functionally graded materials (FGM) used in plates contain probably a porosity volume fraction which needs taking into account this aspect of imperfection in the mechanical bahavior of such structures. The present work aims to study the effect of the distribution forms of porosity on the bending of simply supported FG sandwich plate. The governing equations of the problem are derived by using the principle of virtual work. In the solution of the governing equations, the Navier procedure is used for the simply supported plate. In the porosity effect, four different porosity types are used for functionally graded sandwich plates. In the numerical results, the effects of the porosity parameters, porosity types and aspect ratio of plates on the normal stress, shear stress and static deflections of the functionally graded sandwich plates are presented and discussed. Also, some comparison studies are performed in order to validate the present formulations.

Keywords: functionally graded materials; higher-order plate theory; porosity; sandwich plates

1. Introduction

Functionally graded materials (FGM) are a type of composites whose properties vary gradually though directions. Functionally graded materials have more strength than the classical composites and have not interface problems in contrast with layered composites. Because of these advantages, the functionally graded materials have been investigated for last decade.

In the production stage of the functionally graded materials, micro-voids and porosities could occur due to production or technical errors. This is because of the large difference in solidification temperatures between material constituents (Zhu *et al*. 2001). With porosity, the mechanical behavior of functionally graded materials changes considerably. Thus, the effect of the porosity on the functionally graded materials is an important problem and must be investigated in order to safe design of this composite.

In last years, lots of researchers focus on investigation of porous functionally graded materials; Wattanasakulpong *et al*. (2012) also gave the discussion on porositieshappen ing inside FGM samples fabricated by a multistep sequential infiltration technique. Wattanasakulpong and Ungbhakorn (2014) studied vibration characteristics of FGM porous beams by using differential transformation method with different kinds of elastic supports. Al Jahwari and Naguib (2016) studied the analysis and homogenization of functionally graded viscoelastic porous structures with a higher order plate theory and statistical based model of cellular distribution. Ebrahimi and Jafari (2016) investigated thermal vibration of FGM porous beams. Ebrahimi *et al*. (2016) investigated thermal effects on vibration behavior of temperature-dependent compositionally graded Euler beams with porosities. Kitipornchai *et al*. (2017) studied free vibration and elastic buckling of functionally graded porous beams reinforced by graphene platelets. Wu *et al*. (2018) performed a finite element analysis to study the free and forced vibration FGM porous beam using both Euler-Bernoulli and Timoshenko beam theories. Yang *et al*. (2018) used Chebyshev-Ritz method to study buckling and free vibration of FGM graphene reinforced porous nanocomposite. Şimşek and Aydın investigated size-dependent forced vibration of an imperfect functionally graded (FG) microplate with porosities subjected to a moving load using the modified couple stress theory. Akbaş (2017) examined the vibration

*Corresponding author, Ph.D.,
E-mail: had_laz@yahoo.fr

ISSN: 1738-1584 (Print), 1738-1991 (Online)

and static analysis of functionally graded plates with porosity. Fazzolari (2018) exploited generalized beam theories to study the vibration and stability of porous FGM sandwich beams resting on elastic foundations. Jouneghani *et al*. (2018) studied analytically the structural response of porous FGM nonlocal nanobeams under hygro-thermo-mechanical loadings. Shahsavari *et al*. (2018) used a novel quasi-3D hyperbolic theory for free vibration of FG plates with porosities resting on Winkler/Pasternak/Kerr foundation. Nguyen *et al*. (2018) studied nonlinear dynamic response of functionally graded porous plates on elastic foundation subjected to thermal and mechanical loads. Avcar (2019) examined the free vibration of functionally graded beams with porosity with different porosity distribution models. Ramteke *et al*. (2019) studied effects of the porosity on the eigen characteristics of functionally graded structures with different types of porosity and material distributions. Taati and Fallah (2019) presented forced vibration of sandwich modified strain gradient microbeams with FGM core. Xu *et al*. (2019) studied buckling analysis of functionally graded porous plates with laminated face sheets by using finite element method based on first order shear deformation theory. Zhao *et al*. (2019) investigated vibration behavior of the FGM porous curved thick beam, doubly-curved panels and shells of revolution by using a semi-analytical method. Keddouri *et al*. (2019) presented static responses of functionally graded plates with porosity effects by using the Navier method. Ebrahimi *et al*. (2019) studied vibration analysis of porous metal foam shells rested on an elastic substrate.

Since the shear deformation effects are more pronounced in these structures, the first-order shear deformation theory and higher-order shear deformation theories should be used. By using these theories, although many papers have been devoted to study static, vibration and buckling analysis of FG structures.

In this paper, stress distribution and static deflection of porous functionally graded sandwich plates are investigated with different porosity models by using the Navier method. The higher-order shear deformation plate theory is used in order to get more realistic of stress distribution. The distinctive feature of this study from published papers in the literature is to investigate the porous functionally graded sandwich plates with four porosity types and higher-order shear deformation plate theory. The effects of the porosity parameters, porosity types and aspect ratio of plates on the normal stress, shear stress and static deflections are presented and discussed.

2. Problem formulation

A simply supported sandwich rectangular plate with porous functionally graded face layers is shown in Fig. 1. Where, a, b and h indicate the dimension in the X, Y and Z directions, respectively.

The sandwich plate is made of three layers, an isotropic core and two power-law functionally graded layers. The material properties of the face layers vary from metal to ceramic and the core layer is made of ceramic. The volume fraction $^{(n)}$ of layer n (n = 1, 2, 3), varies according to the following power-law function across the plate thickness

$$V^{(1)}(Z) = \left(\frac{Z - h_1}{h_2 - h_1}\right)^k \; h_1 \le Z \le h_2 \tag{1a}$$

$$V^{(2)}(Z) = 1 \; h_2 \le Z \le h_3 \tag{1b}$$

$$V^{(3)}(Z) = \left(\frac{Z - h_4}{h_3 - h_4}\right)^k \; h_3 \le Z \le h_4 \tag{1c}$$

where h_1, h_2 and h_3 are the bottom surface coordinates of the bottom face layer, the core layer and the top layer respectively. Likewise, h_2, h_3 and h_4 are the top surface coordinates of the bottom face layer, the core layer and the top layer respectively. In equation 1, k indicates the power-law coefficient (volume fraction index). When k = 0, the material of plate gets homogenous ceramic.

In the porosity distribution of functionally graded layers, four different porosity distribution models are used. These porosity distribution models are shown in Fig. 2. Used the porosity models in this study are; homogeneous porosity distribution, X porosity distribution, O porosity distribution and V porosity distribution.

According to these models, the effective material properties (P) for each layers are given as follows (Hadji and Avcar 2021);

For Homogeneous Porosity Distribution

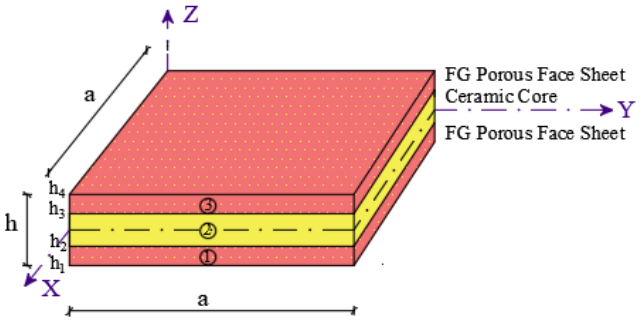

Fig. 1 Geometry of a simply supported sandwich rectangular plate with functionally graded porous layers

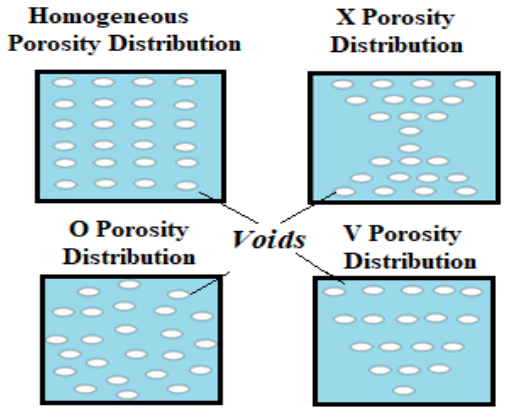

Fig. 2 Porosity distribution models

$$\begin{cases} P^{(1)}(z) = P_m + (P_c - P_m)V^{(1)}(z) - \dfrac{\alpha}{2}(P_c + P_m) \\ P^{(2)}(z) = P_m + (P_c - P_m)V^{(2)}(z) \\ P^{(3)}(z) = P_m + (P_c - P_m)V^{(3)}(z) - \dfrac{\alpha}{2}(P_c + P_m) \end{cases} \quad (2)$$

$$\begin{Bmatrix} \varepsilon_x \\ \varepsilon_y \\ \gamma_{xy} \end{Bmatrix} = \begin{Bmatrix} \varepsilon_x^0 \\ \varepsilon_y^0 \\ \gamma_{xy}^0 \end{Bmatrix} + z \begin{Bmatrix} k_x^b \\ k_y^b \\ k_{xy}^b \end{Bmatrix} + f(z) \begin{Bmatrix} k_x^s \\ k_y^s \\ k_{xy}^s \end{Bmatrix}, \quad (8a)$$

For X Porosity Distribution

$$\begin{cases} P^{(1)}(z) = P_m + (P_c - P_m)V^{(1)}(z) - \dfrac{\alpha}{2}(P_c + P_m)\left|\dfrac{2z - (h_1 + h_2)}{h_1 - h_2}\right| \\ P^{(2)}(z) = P_m + (P_c - P_m)V^{(2)}(z) \\ P^{(3)}(z) = P_m + (P_c - P_m)V^{(3)}(z) - \dfrac{\alpha}{2}(P_c + P_m)\left|\dfrac{2z - (h_3 + h_4)}{h_3 - h_4}\right| \end{cases} \quad (3)$$

For O Porosity Distribution

$$\begin{cases} P^{(1)}(z) = P_m + (P_c - P_m)V^{(1)}(z) - \dfrac{\xi}{2}(P_c + P_m)\sqrt{\left(\dfrac{h_1 - h_2}{2}\right)^2 - \left(z - \left(\dfrac{h_1 + h_2}{2}\right)\right)^2} \\ P^{(2)}(z) = P_m + (P_c - P_m)V^{(2)}(z) \\ P^{(3)}(z) = P_m + (P_c - P_m)V^{(3)}(z) - \dfrac{\xi}{2}(P_c + P_m)\sqrt{\left(\dfrac{h_3 - h_4}{2}\right)^2 - \left(z - \left(\dfrac{h_3 + h_4}{2}\right)\right)^2} \end{cases} \quad (4)$$

For V Porosity Distribution

$$\begin{cases} P^{(1)}(z) = P_m + (P_c - P_m)V^{(1)}(z) - \dfrac{\alpha}{2}(P_c + P_m)\left(\dfrac{z - h_2}{h_1 - h_2}\right) \\ P^{(2)}(z) = P_m + (P_c - P_m)V^{(2)}(z) \\ P^{(3)}(z) = P_m + (P_c - P_m)V^{(3)}(z) - \dfrac{\alpha}{2}(P_c + P_m)\left(\dfrac{z - h_4}{h_3 - h_4}\right) \end{cases} \quad (5)$$

where α ($\alpha \prec 1$) demotes the volume fraction of porosity.

Based on the higher-order shear deformation plate theory, the displacement fields of the plate are presented as follows

$$\begin{aligned} u(x,y,z,t) &= u_0(x,y,t) - z\frac{\partial w_0}{\partial x} \\ &\quad + k_1 f(z)\int \theta(x,y,t)\,dx \\ v(x,y,z,t) &= v_0(x,y,t) - z\frac{\partial w_0}{\partial y} \\ &\quad + k_2 f(z)\int \theta(x,y,t)\,dy \\ w(x,y,z,t) &= w_0(x,y,t) \end{aligned} \quad (6)$$

Where, *u*, *v* and *w* are the displacements functions of *X*, *Y* and *Z* directions, respectively. In Eq. (6), *f*(z) is defined according to the higher-order shear deformation plate as follows (Akavci 2010)

$$f(z) = \frac{3}{2}\pi h \tanh\left(\frac{z}{h}\right) - \frac{3}{2}\pi z \operatorname{sec} h\left(\frac{1}{2}\right)^2 \quad (7)$$

It can be seen that the displacement field in Eq. (6) introduces only four unknowns (u_0,v_0,w_0 and θ). The nonzero strains associated with the displacement field in Eq. (6) are

$$\begin{Bmatrix} \gamma_{yz} \\ \gamma_{xz} \end{Bmatrix} = g(z) \begin{Bmatrix} \gamma_{yz}^0 \\ \gamma_{xz}^0 \end{Bmatrix}, \quad (8b)$$

where

$$\begin{Bmatrix} \varepsilon_x^0 \\ \varepsilon_y^0 \\ \gamma_{xy}^0 \end{Bmatrix} = \begin{Bmatrix} \dfrac{\partial u_0}{\partial x} \\ \dfrac{\partial v_0}{\partial x} \\ \dfrac{\partial u_0}{\partial y} + \dfrac{\partial v_0}{\partial x} \end{Bmatrix}, \quad \begin{Bmatrix} k_x^b \\ k_y^b \\ k_{xy}^b \end{Bmatrix} = \begin{Bmatrix} -\dfrac{\partial^2 w_0}{\partial x^2} \\ -\dfrac{\partial^2 w_0}{\partial y^2} \\ -2\dfrac{\partial^2 w_0}{\partial x \partial y} \end{Bmatrix} \quad (9a)$$

$$\begin{Bmatrix} k_x^s \\ k_y^s \\ k_{xy}^s \end{Bmatrix} = \begin{Bmatrix} k_1\theta \\ k_2\theta \\ k_1\dfrac{\partial}{\partial y}\int \theta\,dx + k_2\dfrac{\partial}{\partial x}\int \theta\,dy \end{Bmatrix}, \quad \begin{Bmatrix} \gamma_{yz}^0 \\ \gamma_{xz}^0 \end{Bmatrix} = \begin{Bmatrix} k_2\int \theta\,dy \\ k_1\int \theta\,dx \end{Bmatrix} \quad (9b)$$

and

$$g(z) = \frac{df(z)}{dz} \quad (10)$$

The integrals defined in the above equations shall be

resolved by a Navier type method and can be written as follows

$$\frac{\partial}{\partial y}\int \theta\, dx = A'\frac{\partial^2\theta}{\partial x\partial y}, \quad \frac{\partial}{\partial x}\int \theta\, dy = B'\frac{\partial^2\theta}{\partial x\partial y}, \quad \int \theta\, dx = A'\frac{\partial\theta}{\partial x}, \quad \int \theta\, dy = B'\frac{\partial\theta}{\partial y} \tag{11}$$

where the coefficients A' and B' are expressed according to the type of solution used, in this case via Navier. Therefore, A', B', k_1 and k_2 are expressed as follows

$$A' = -\frac{1}{\alpha^2}, \quad B' = -\frac{1}{\beta^2}, \quad k_1 = \alpha^2, \quad k_2 = \beta^2 \tag{12}$$

where α and β are defined in expression (28). For elastic and isotropic FGMs, the constitutive relations can be expressed as

$$\begin{Bmatrix}\sigma_x\\ \sigma_y\\ \tau_{xy}\\ \tau_{yz}\\ \tau_{xz}\end{Bmatrix} = \begin{bmatrix}C_{11} & C_{12} & 0 & 0 & 0\\ C_{12} & C_{22} & 0 & 0 & 0\\ 0 & 0 & C_{66} & 0 & 0\\ 0 & 0 & 0 & C_{44} & 0\\ 0 & 0 & 0 & 0 & C_{55}\end{bmatrix}\begin{Bmatrix}\varepsilon_x\\ \varepsilon_y\\ \gamma_{xy}\\ \gamma_{yz}\\ \gamma_{xz}\end{Bmatrix} \tag{13}$$

where (σ_x, σ_y, τ_{xy}, τ_{yz}, τ_{xz}) and (ε_x, ε_y, γ_{xy}, γ_{yz}, γ_{xz}) are the stress and strain components, respectively. Using the material properties defined in Eq. (1), stiffness coefficients, C_{ij}, can be given as

$$C_{11} = C_{22} = \frac{E(z)}{1-v^2}, C_{12} = \frac{vE(z)}{1-v^2}, \quad C_{44} = C_{55} = C_{66} = \frac{E(z)}{2(1+v)}, \tag{14}$$

The governing equations of equilibrium can be derived by using the principle of virtual displacements. The principle of virtual work in the present case yields (Merazi *et al*. 2015)

$$\int_{-h/2}^{h/2}\int_{\Omega}\begin{bmatrix}\sigma_x\delta\varepsilon_x + \sigma_y\delta\varepsilon_y + \tau_{xy}\delta\gamma_{xy}\\ +\tau_{xz}\delta\gamma_{xz} + \tau_{yz}\delta\gamma_{yz}\end{bmatrix} d\Omega dz - \int_{\Omega} q(x,y)\,\delta w d\Omega = 0 \tag{15}$$

where Ω is the top surface and $q(x,y)$ is the applied transverse load.

Substituting Eqs. (8) and (13) into Eq. (15) and integrating through the thickness of the plate, Eq. (15) can be rewritten as

$$\int_{\Omega}\begin{bmatrix}N_x\delta\varepsilon_x^0 + N_y\delta\varepsilon_y^0 + N_{xy}\delta\gamma_{xy}^0 + M_x^b\delta k_x^b\\ +M_y^b\delta k_y^b + M_{xy}^b\delta k_{xy}^b + M_x^s\delta k_x^s + M_y^s\delta k_y^s\\ +M_{xy}^s\delta k_{xy}^s + S_{yz}^s\delta\gamma_{yz}^0 + S_{xz}^s\delta\gamma_{xz}^0\end{bmatrix} d\Omega - \int_{\Omega} q\delta w d\Omega = 0, \tag{16}$$

The stress resultants N, M, and S are defined by

$$\left(N_i, M_i^b, M_i^s\right) = \int_{-\frac{h}{2}}^{\frac{h}{2}}(1, z, f)\sigma_i dz\,, (i = x, y, xy) \quad \text{and} \quad \left(S_{xz}^s, S_{yz}^s\right) = \int_{-h/2}^{h/2} g\left(\tau_{xz}, \tau_{yz}\right)dz \tag{17}$$

The governing equations of equilibrium can be derived from Eq. (16) by integrating the displacement gradients by parts and setting the coefficients zero δu_0, δv_0, δw_0, and $\delta\theta$ separately. Thus, one can obtain the equilibrium equations associated with the present refined shear deformation plate theory

$$\begin{aligned}
&\delta u_0: \ \frac{\partial N_x}{\partial x} + \frac{\partial N_{xy}}{\partial y} = 0\\
&\delta v_0: \ \frac{\partial N_{xy}}{\partial x} + \frac{\partial N_y}{\partial y} = 0\\
&\delta w_0: \ \frac{\partial^2 M_x^b}{\partial x^2} + 2\frac{\partial^2 M_{xy}^b}{\partial x\partial y} + \frac{\partial^2 M_y^b}{\partial y^2} + q = 0\\
&\delta\theta: \ -k_1 M_x^s - k_2 M_y^s - (k_1 A' + k_2 B')\frac{\partial^2 M_{xy}^s}{\partial x\partial y}\\
&\qquad k_1 A'\frac{\partial S_{xz}^s}{\partial x} + k_2 B'\frac{\partial S_{yz}^s}{\partial y} = 0
\end{aligned} \tag{18}$$

Substituting Eq. (8) into Eq. (13) and the subsequent results into Eqs. (17), the stress resultants are obtained in terms of strains as following compact form

$$\begin{Bmatrix}N\\ M^b\\ M^s\end{Bmatrix} = \begin{bmatrix}A & B & B^s\\ B & D & D^s\\ B^s & D^s & H^s\end{bmatrix}\begin{Bmatrix}\varepsilon\\ k^b\\ k^s\end{Bmatrix}, \qquad S = A^s\gamma, \tag{19}$$

in which

$$N = \left\{N_x, N_y, N_{xy}\right\}^t, \quad M^b = \left\{M_x^b, M_y^b, M_{xy}^b\right\}^t, \quad M^s = \left\{M_x^s, M_y^s, M_{xy}^s\right\}^t \tag{20a}$$

$$\varepsilon = \left\{\varepsilon_x^0, \varepsilon_y^0, \gamma_{xy}^0\right\}^t, \quad k^b = \left\{k_x^b, k_y^b, k_{xy}^b\right\}^t, \quad k^s = \left\{k_x^s, k_y^s, k_{xy}^s\right\}^t \tag{20b}$$

$$A = \begin{bmatrix}A_{11} & A_{12} & 0\\ A_{12} & A_{22} & 0\\ 0 & 0 & A_{66}\end{bmatrix}, \quad B = \begin{bmatrix}B_{11} & B_{12} & 0\\ B_{12} & B_{22} & 0\\ 0 & 0 & B_{66}\end{bmatrix}, \quad D = \begin{bmatrix}D_{11} & D_{12} & 0\\ D_{12} & D_{22} & 0\\ 0 & 0 & D_{66}\end{bmatrix} \tag{20c}$$

$$B^s = \begin{bmatrix}B_{11}^s & B_{12}^s & 0\\ B_{12}^s & B_{22}^s & 0\\ 0 & 0 & B_{66}^s\end{bmatrix}, \quad D^s = \begin{bmatrix}D_{11}^s & D_{12}^s & 0\\ D_{12}^s & D_{22}^s & 0\\ 0 & 0 & D_{66}^s\end{bmatrix}, \quad H^s = \begin{bmatrix}H_{11}^s & H_{12}^s & 0\\ H_{12}^s & H_{22}^s & 0\\ 0 & 0 & H_{66}^s\end{bmatrix} \tag{20d}$$

$$S=\{S_{xz}^s, S_{yz}^s\}^t, \qquad \gamma=\{\gamma_{xz}^0, \gamma_{yz}^0\}^t,$$
$$A^s=\begin{bmatrix} A_{44}^s & 0 \\ 0 & A_{55}^s \end{bmatrix} \tag{20e}$$

and stiffness components are given as

$$\begin{Bmatrix} A_{11} & B_{11} & D_{11} & B_{11}^s & D_{11}^s & H_{11}^s \\ A_{12} & B_{12} & D_{12} & B_{12}^s & D_{12}^s & H_{12}^s \\ A_{66} & B_{66} & D_{66} & B_{66}^s & D_{66}^s & H_{66}^s \end{Bmatrix} \tag{21a}$$

$$=\int_{-h/2}^{h/2} C_{11}(1, z, z^2, f(z), z\,f(z), f^2(z)) \begin{Bmatrix} 1 \\ \nu \\ \dfrac{1-\nu}{2} \end{Bmatrix} dz \tag{21b}$$

$$(A_{22}, B_{22}, D_{22}, B_{22}^s, D_{22}^s, H_{22}^s) = (A_{11}, B_{11}, D_{11}, B_{11}^s, D_{11}^s, H_{11}^s) \tag{21c}$$

$$A_{44}^s = A_{55}^s = \int_{-h/2}^{h/2} C_{44}[g(z)]^2 dz, \tag{21d}$$

In what follows, the problem under consideration is solved for the following simply supported boundary conditions prescribed at all four edges

$$v_0(0,y) = w_b(0,y) = w_s(0,y) = \frac{\partial w_b}{\partial y}(0,y) = \frac{\partial w_s}{\partial y}(0,y) = 0 \tag{22a}$$

$$v_0(a,y) = w_b(a,y) = w_s(a,y) = \frac{\partial w_b}{\partial y}(a,y) = \frac{\partial w_s}{\partial y}(a,y) = 0 \tag{22b}$$

$$N_x(0,y) = M_x^b(0,y) = M_x^s(0,y) = N_x(a,y) = M_x^b(a,y) = M_x^s(a,y) = 0 \tag{22c}$$

$$u_0(x,0) = w_b(x,0) = w_s(x,0) = \frac{\partial w_b}{\partial y}(x,0) = \frac{\partial w_s}{\partial y}(x,0) = 0 \tag{22d}$$

$$u_0(x,0) = w_b(x,b) = w_s(x,b) = \frac{\partial w_b}{\partial y}(x,b) = \frac{\partial w_s}{\partial y}(x,b) = 0 \tag{22e}$$

$$N_y(x,0) = M_y^b(x,0) = M_y^s(x,0) = N_y(x,b) = M_y^b(x,b) = M_y^s(x,b) = 0 \tag{22f}$$

Introducing Eq. (19) into Eq. (18), the equations of motion can be expressed in terms of displacements (u_0, v_0, w_0, θ) and the appropriate equations take the form

$$\begin{aligned} &A_{11}d_{11}u_0 + A_{66}d_{22}u_0 + (A_{12}+A_{66})d_{12}v_0 \\ &-B_{11}d_{111}w_0 - (B_{12}+2B_{66})d_{122}w_0 \\ &+\big(B_{66}^s(k_1A' + k_2B')\big)d_{122}\theta + (B_{11}^s k_1 + B_{12}^s k_2)d_1\theta \\ &= 0, \end{aligned} \tag{23a}$$

$$\begin{aligned} &A_{22}d_{22}v_0 + A_{66}d_{11}v_0 + (A_{12}+A_{66})d_{12}u_0 \\ &-B_{22}d_{222}w_0 - (B_{12}+2B_{66})d_{112}w_0 \\ &+\big(B_{66}^s(k_1A' + k_2B')\big)d_{112}\theta + (B_{22}^s k_2 + B_{12}^s k_1)d_2\theta \\ &= 0, \end{aligned} \tag{23b}$$

$$\begin{aligned} &B_{11}d_{111}u_0 + (B_{12}+2B_{66})d_{122}u_0 \\ &+(B_{12}+2B_{66})d_{112}v_0 + B_{22}d_{222}v_0 \\ &-D_{11}d_{1111}w_0 - 2(D_{12}+2D_{66})d_{1122}w_0 \\ &-D_{22}d_{2222}w_0 + (D_{11}^s k_1 + D_{12}^s k_2)d_{11}\theta \\ &+2\big(D_{66}^s(k_1A' + k_2B')\big)d_{1122}\theta \\ &+(D_{12}^s k_1 + D_{22}^s k_2)d_{22}\theta + q = 0 \end{aligned} \tag{23c}$$

$$\begin{aligned} &-(B_{11}^s k_1 + B_{12}^s k_2)d_1u_0 - \big(B_{66}^s(k_1A' + k_2B')\big)d_{122}u_0 \\ &-\big(B_{66}^s(k_1A' + k_2B')\big)d_{112}v_0 - (B_{12}^s k_1 + B_{22}^s k_2)d_2v_0 \\ &+(D_{11}^s k_1 + D_{12}^s k_2)d_{11}w_0 \\ &+2\big(D_{66}^s(k_1A' + k_2B')\big)d_{1122}w_0 \\ &+(D_{12}^s k_1 + D_{22}^s k_2)d_{22}w_0 \\ &-H_{11}^s k_1^2\theta - H_{22}^s k_2^2\theta - 2H_{12}^s k_1 k_2\theta \\ &-((k_1A' + k_2B')^2 H_{66}^s)d_{1122}\theta + A_{44}^s(k_2B')^2 d_{22}\theta \\ &+A_{55}^s(k_1A')^2 d_{11}\theta = 0 \end{aligned} \tag{23d}$$

where d_{ij}, d_{ijl} and d_{ijlm} are the following differential operators

$$d_{ij} = \frac{\partial^2}{\partial x_i \partial x_j}, \qquad d_{ijl} = \frac{\partial^3}{\partial x_i \partial x_j \partial x_l},$$
$$d_{ijlm} = \frac{\partial^4}{\partial x_i \partial x_j \partial x_l \partial x_m}, \quad d_i = \frac{\partial}{\partial x_i} \tag{24}$$
$$(i,j,l,m = 1,2).$$

The Navier solution technique is a well-established approach utilizing a series solution expansion of the kinematic field. However, there exists alternative solution approach in the literature based on the series expansion of the kinetic field (Farrahi *et al*. 2009, Faghidian 2014, 2015). In this paper the Navier solution method is employed to determine the analytical solutions for which the displacement variables are written as product of arbitrary parameters and known trigonometric functions to respect the equations of motion and boundary conditions.

The displacement functions that satisfy the equations of boundary conditions (22) are selected as the following Fourier series

$$\begin{Bmatrix} u_0 \\ v_0 \\ w_0 \\ \theta \end{Bmatrix} = \sum_{m=1}^{\infty}\sum_{n=1}^{\infty} \begin{Bmatrix} U_{mn}\cos(\alpha x)\sin(\beta y) \\ V_{mn}\sin(\alpha x)\cos(\beta y) \\ W_{mn}\sin(\alpha x)\sin(\beta y) \\ X_{mn}\sin(\alpha x)\sin(\beta y) \end{Bmatrix} \tag{25}$$

with

$$\alpha = \frac{m\pi}{a} \quad \text{and} \quad \beta = n\pi/b \tag{26}$$

The transverse uniform distributed load q is also expanded in the double-Fourier sine series as

$$q(x,y) = \sum_{m=1}^{\infty}\sum_{n=1}^{\infty} Q_{mn}\sin(\alpha x)\sin(\beta y), \tag{27}$$

where

$$Q_{mn} = \frac{4}{ab}\int_0^a\int_0^b q(x,y)\sin(\alpha x)\sin(\beta y)\,dxdy = \begin{cases} q_0 \text{ for sinusoidally distributed load} \\ \dfrac{16q_0}{mn\pi^2} \text{ for uniformly distributed load} \end{cases} \tag{28}$$

Substituting Eqs. (25) and (27) into Eq. (22), the following problem is obtained

$$\begin{bmatrix} S_{11} & S_{12} & S_{13} & S_{14} \\ S_{12} & S_{22} & S_{23} & S_{24} \\ S_{13} & S_{23} & S_{33} & S_{34} \\ S_{14} & S_{24} & S_{34} & S_{44} \end{bmatrix} \begin{Bmatrix} U_{mn} \\ V_{mn} \\ W_{mn} \\ W_{mn} \end{Bmatrix} = \begin{Bmatrix} 0 \\ 0 \\ Q_{mn} \\ 0 \end{Bmatrix} \tag{29}$$

where

$$\begin{aligned} S_{11} &= -(A_{11}\alpha^2 + A_{66}\beta^2), \\ S_{12} &= -\alpha\beta(A_{12} + A_{66}), \\ S_{13} &= \alpha(B_{11}\alpha^2 + B_{12}\beta^2 + 2B_{66}\beta^2), \\ S_{14} &= \alpha(k_1 B_{11}^s + k_2 B_{12}^s - (k_1 A' + k_2 B')B_{66}^s\beta^2), \\ S_{22} &= -(A_{66}\alpha^2 + A_{22}\beta^2), \\ S_{23} &= \beta(B_{22}\beta^2 + B_{12}\alpha^2 + 2B_{66}\alpha^2), \\ S_{24} &= \beta(k_2 B_{22}^s + k_1 B_{12}^s - (k_1 A' + k_2 B')B_{66}^s\alpha^2), \end{aligned} \tag{30}$$

3. Numerical results

In this section, effects of the porosity distributions, the porosity parameters, the aspect ratios of plates on the normal stress, shear stress and static deflections of the functionally graded sandwich plates are presented and discussed under transverse uniform distributed load (q_0). Unless mentioned otherwise, a simply supported Al/ZrO_2 sandwich plate composed of Aluminum face sheets (as metal) and Zirconia core (as ceramic) under sinusoidal loads is considered. Young's modulus and Poisson's ratio of Aluminum are E_m = 70 GPa, ν_m = 0.3 respectively, and those of Zirconia are E_c = 151 GPa, ν_c = 0.3.

Numerical results are presented in terms of non-dimensional stresses and deflection. The various nondimensional parameters used are

- Dimensionless deflection: $\hat{w} = \frac{10hE_0}{q_0 a^2} w\left(\frac{a}{2}, \frac{b}{2}\right)$,
- Dimensionless normal stress: $\overline{\sigma}_x = \frac{10.h^2}{q_0 a^2}\sigma_x\left(\frac{a}{2}, \frac{b}{2}, z\right)$,
- Dimensionless transverse shear stress: $\overline{\tau}_{xz} = \frac{h}{q_0 a}\tau_{xz}\left(0, \frac{b}{2}, z\right)$.

where E_0 = 1 GPa. It is noted that the deflections are calculated at the $X = a/2$, $Y = b/2$, the distribution of axial stress is presented at the cross section $X = a/2$, $Y = b/2$ in though Z direction and the distribution of shear stress is presented at the cross section $X = 0$, $Y = b/2$ in though Z direction. Several kinds of symmetric and non-symmetric FGM sandwich plate are used as follows;

The (1-0-1) FGM sandwich plate: The plate is made of two layers of equal thickness without a core:

$$h_1 = h_3 = h/2, \qquad h_2 = 0$$

The (1-1-1) FGM sandwich plate: The plate is made of three equal-thickness layers:

$$h_1 = h_2 = h_3 = h/3$$

The (1-2-1) FGM sandwich plate: The core thickness equals the sum of faces thickness:

$$h_1 = h_3 = h/4, \qquad h_2 = h/2$$

The (2-1-2) FGM sandwich plate: The upper layer thickness is twice the core layer while it is the same as the lower one:

$$h_1 = h_3 = 2h/5, \qquad h_2 = h/5$$

The (2-2-1) FGM sandwich plate: The core thickness is twice the upper face while it is the same as the lower one.

$$h_1 = h_2 = 2h/5, \qquad h_3 = h/5$$

In order to prove the validity of the presentedhigher-order shear deformation plate theory, some comparisons are made between the results obtained from this theory and those obtained by Zenkour (2005) based on sinusoidal shear deformation theory (SSDPT), trigonometric shear deformation theory (TSDPT), the first-order shear deformation theory (FSDPT) and the new first-order shear deformation developed by Thai *et al*. (2014) as given in Tables 1 to 3.

From these tables, a good agreement between the results of the present theory with other theories except for the case of transverse shear stress τ_{xz}. A small difference between the results is seen (see Table 3). This is due to the different approaches used to predict the transverse shear stresses. It is clear that the FSDPT (Zenkour 2005) violates the stress-free boundary conditions on the plate surface, and consequently, a shear correction factor is required. Finally, it is important to note that the present theory involves only four unknowns as against five in the case of SSDT, TSDT and FSDT. Besides, it does not require a shear correction factor as in the case of FSDT. Therefore, it can be stated that the present theory is not only accurate but also simple in predicting the bending behavior of FG sandwich plates.

Fig. 3 indicates the effect the side-to-thickness ratio a/h and the shape of porosity distribution on the dimensionless deflections $\hat{w}$ of (1-1-1) sandwich plates with different value of volume fraction k and porosity coefficient α = 0.2. The deflections for plate with uniform porosity distribution model are higher than that for the other models of imperfect FGM sandwich plates. The highest values of dimensionless deflections were obtained for the homogeneous shape of porosity distribution while the lowest ones correspond to the "O" shape of porosity distribution. The "*X*" and the "*V*" shape of porosity distribution gives almost the same values of the dimensionless deflections. It is seen from Fig. 3, the dimensionless deflections increase with the increasing of the side-to-thickness ratio a/h. Another result of Fig. 3 is that the difference among of porosity distributions increase significantly by increasing the ratio of a/h. In higher values of a/h, the porosity is very effective on the static behavior of FGM sandwich plates. It should be noted that the effect of the distribution shape of porosity on the dimensionless deflection is very significant by increasing thickness ratio. Also, the value of volume fraction (k) is very effective on the porosity and its influences. By increasing the value of volume fraction, the difference among of porosity distributions increases.

Table 1 Dimensionless deflection $\hat{w}$ of square plates for $a/h = 10$

k	Theory	Scheme			
		1-0-1	2-1-2	1-1-1	2-2-1
0	SSDPT (Zenkour, 2005)	0.1961	0.1961	0.1961	0.1961
	TSDPT (Zenkour, 2005)	0.1961	0.1961	0.1961	0.1961
	FSDPT (Zenkour, 2005)	0.1961	0.1961	0.1961	0.1961
	NFSDPT (Thai, 2014)	0.1961	0.1961	0.1961	0.1961
	Present	0.1961	0.1961	0.1961	0.1961
1	SSDPT (Zenkour, 2005)	0.3235	0.3062	0.2919	0.2808
	TSDPT (Zenkour, 2005)	0.3236	0.3063	0.2920	0.2809
	FSDPT (Zenkour, 2005)	0.3248	0.3075	0.2930	0.2817
	NFSDPT (Thai, 2014)	0.3237	0.3064	0.2920	0.2809
	Present	0.3235	0.3063	0.2919	0.2802
2	SSDPT (Zenkour, 2005)	0.3732	0.3522	0.3328	0.3161
	TSDPT (Zenkour, 2005)	0.3734	0.3523	0.3329	0.3162
	FSDPT (Zenkour, 2005)	0.3751	0.3541	0.3344	0.3174
	NFSDPT (Thai, 2014)	0.3737	0.3526	0.3330	0.3163
	Present	0.3732	0.3522	0.3328	0.3149
5	SSDPT (Zenkour, 2005)	0.4091	0.3916	0.3713	0.3495
	TSDPT (Zenkour, 2005)	0.4093	0.3918	0.3715	0.3496
	FSDPT (Zenkour, 2005)	0.4112	0.3942	0.3736	0.3512
	NFSDPT (Thai, 2014)	0.4101	0.3927	0.3720	0.3501
	Present	0.4091	0.3917	0.3713	0.3476
10	SSDPT (Zenkour, 2005)	0.4175	0.4037	0.3849	0.3492
	TSDPT (Zenkour, 2005)	0.4177	0.4041	0.3855	0.3622
	FSDPT (Zenkour, 2005)	0.4192	0.4066	0.3879	0.3640
	NFSDPT (Thai, 2014)	0.3988	0.3894	0.3724	0.3492
	Present	0.4176	0.4039	0.3854	0.3598

Table 2 Dimensionless normal stress $\overline{\sigma}_x(h/2)$ of square plates for $a/h = 10$

k	Theory	Scheme			
		1-0-1	2-1-2	1-1-1	2-2-1
0	SSDPT (Zenkour, 2005)	2.0545	2.0545	2.0545	2.0545
	TSDPT (Zenkour, 2005)	2.0499	2.0499	2.0499	2.0499
	FSDPT (Zenkour, 2005)	1.9758	1.9758	1.9758	1.9758
	NFSDPT (Thai, 2014)	1.9758	1.9758	1.9758	1.9758
	Present	1.9951	1.9951	1.9951	1.9951
1	SSDPT (Zenkour, 2005)	1.5820	1.4986	1.4289	1.3234
	TSDPT (Zenkour, 2005)	1.5792	1.4959	1.4262	1.3206
	FSDPT (Zenkour, 2005)	1.5325	1.4517	1.3830	1.2775
	NFSDPT (Thai, 2014)	1.5324	1.4517	1.3830	1.2775
	Present	1.5447	1.4632	1.3943	1.2744
2	SSDPT (Zenkour, 2005)	1.8245	1.7241	1.6303	1.4739
	TSDPT (Zenkour, 2005)	1.8217	1.7214	1.6275	1.4710
	FSDPT (Zenkour, 2005)	1.7709	1.6750	1.5824	1.4253
	NFSDPT (Thai, 2014)	1.7709	1.6750	1.5824	1.4253
	Present	1.7841	1.6871	1.5942	1.4145

Table 2 Continued

k	Theory	Scheme			
		1-0-1	2-1-2	1-1-1	2-2-1
5	SSDPT (Zenkour, 2005)	1.9957	1.9155	1.8184	1.6148
	TSDPT (Zenkour, 2005)	1.9927	1.9130	1.8158	1.6118
	FSDPT (Zenkour, 2005)	1.9358	1.8648	1.7699	1.5640
	NFSDPT (Thai, 2014)	1.9358	1.8648	1.7699	1.5640
	Present	1.9505	1.8773	1.7818	1.5452
10	SSDPT (Zenkour, 2005)	2.0336	1.9731	1.8815	1.6198
	TSDPT (Zenkour, 2005)	2.0304	1.9713	1.8838	1.6666
	FSDPT (Zenkour, 2005)	1.9678	1.9217	1.8375	1.6165
	NFSDPT (Thai, 2014)	1.9678	1.9216	1.8375	1.6160
	Present	1.9841	1.9345	1.8495	1.5944

Table 3 Dimensionless transverse shear stress $\bar{\tau}_{xz}(0)$ of square plates for $a/h = 10$

k	Theory	Scheme			
		1-0-1	2-1-2	1-1-1	2-2-1
0	SSDPT (Zenkour, 2005)	0.2462	0.2462	0.2462	0.2462
	TSDPT (Zenkour, 2005)	0.2386	0.2386	0.2386	0.2386
	FSDPT (Zenkour, 2005)	0.1910	0.1910	0.1910	0.1910
	NFSDPT (Thai, 2014)	0.2387	0.2387	0.2387	0.2387
	Present	0.2441	0.2441	0.2441	0.2441
1	SSDPT (Zenkour, 2005)	0.2991	0.2777	0.2681	0.2668
	TSDPT (Zenkour, 2005)	0.2920	0.2710	0.2612	0.2595
	FSDPT (Zenkour, 2005)	0.2610	0.2432	0.2326	0.2276
	NFSDPT (Thai, 2014)	0.2566	0.2593	0.2602	0.2582
	Present	0.2971	0.2759	0.2662	0.2648
2	SSDPT (Zenkour, 2005)	0.3329	0.2942	0.2781	0.2763
	TSDPT (Zenkour, 2005)	0.3262	0.2884	0.2719	0.2694
	FSDPT (Zenkour, 2005)	0.2973	0.2675	0.2508	0.2432
	NFSDPT (Thai, 2014)	0.2552	0.2617	0.2650	0.2624
	Present	0.3311	0.2926	0.2764	0.2745
5	SSDPT (Zenkour, 2005)	0.3937	0.3193	0.2915	0.2890
	TSDPT (Zenkour, 2005)	0.3863	0.3145	0.2864	0.2827
	FSDPT (Zenkour, 2005)	0.3454	0.2973	0.2721	0.2610
	NFSDPT (Thai, 2014)	0.2468	0.2576	0.2649	0.2627
	Present	0.3917	0.3180	0.2901	0.2874
10	SSDPT (Zenkour, 2005)	0.4415	0.3364	0.2953	0.2967
	TSDPT (Zenkour, 2005)	0.4321	0.3324	0.2957	0.2908
	FSDPT (Zenkour, 2005)	0.3728	0.3132	0.2830	0.2700
	NFSDPT (Thai, 2014)	0.2419	0.2534	0.2627	0.2611
	Present	0.4389	0.3357	0.2989	0.2955

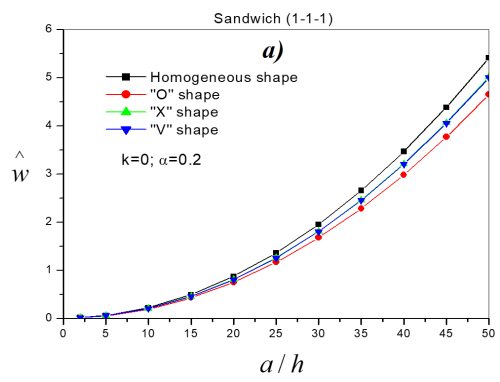

(a) for $k = 0$

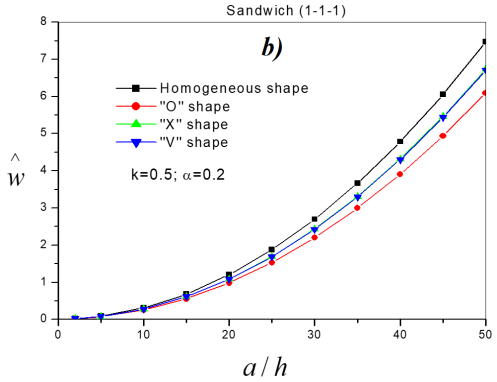

(b) for $k = 0.5$

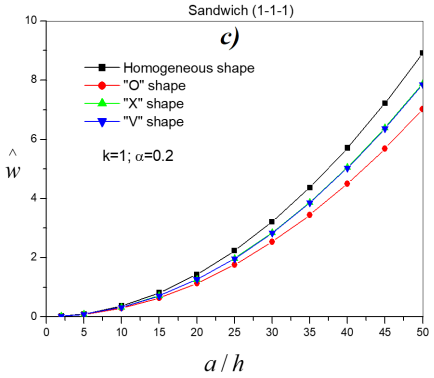

(c) for $k = 1$

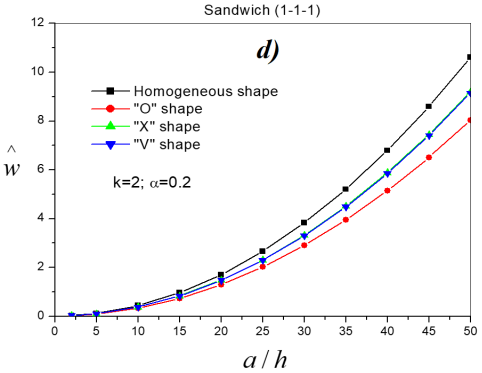

(d) for $k = 2$

Fig. 3 Effect of the shape of porosity distribution on the dimensionless deflections versus side-to-thickness ratio a/h of an Al/ZrO_2 FGM square sandwich plate (1-1-1)

Fig. 4 shows the influence of distribution shape of porosity on the axial stress with different value of volume fraction k and porosity coefficient $\alpha = 0.2$ respectively. It is clair that the axial stress is tensile at the top surface and compressive at the bottom surface. Also, it is clear that the longitudinal stress is maximum for "V" distribution shape of porosity and it is minimal for "X" distribution shape of porosity.

Fig. 5 shows the influence of distribution shape of porosity on the shear stress with different value of volume fraction k and porosity coefficient $\alpha = 0.2$ respectively. It is noted that the variation of the shear stresses is not parabolic. It is clear that the axial stress is maximum for the homogeneous shape of porosity distribution and it is minimal for "O" distribution shape of porosity. It can be also noted that the distribution shape of porosity has an influence on the shear stress.

The axial stress and shear stress are continuous and smooth through the plate sandwich thickness for "O" shape of porosity distribution and non-smooth for homogeneous, X and V shape of porosity distribution.

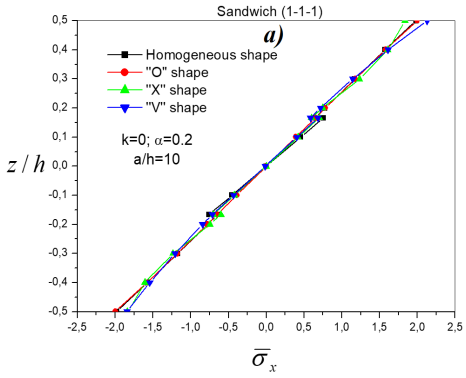

(a) for $k = 0$

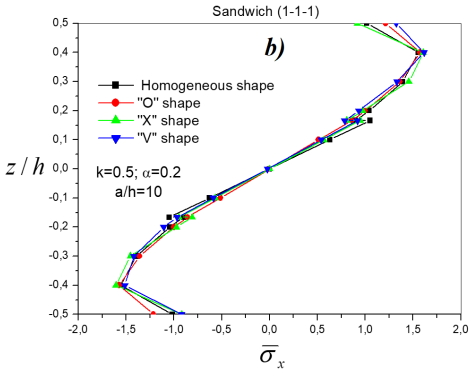

(b) for $k = 0.5$

Fig. 4 Effect of the shape of porosity distribution on the normal stress $\overline{\sigma}_x$ across the thickness of an Al/ZrO_2 FGM square sandwich plate (1-1-1)

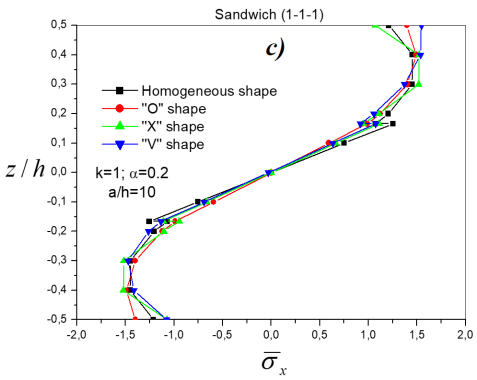

(c) for $k = 1$

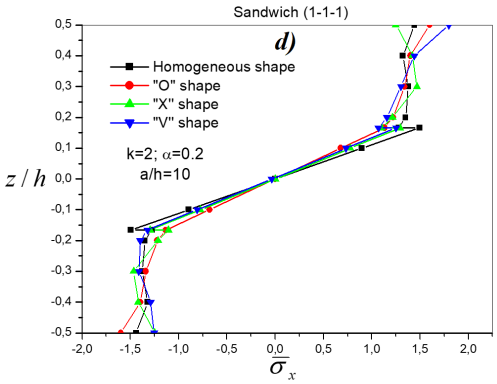

(d) for $k = 2$

Fig. 4 Continued

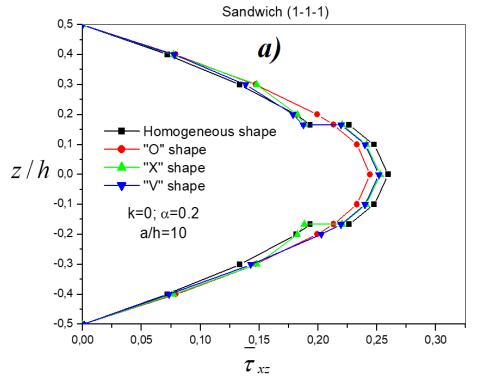

(a) for $k = 0$

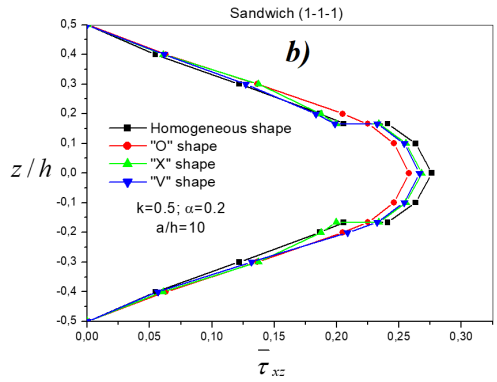

(b) for $k = 0.5$

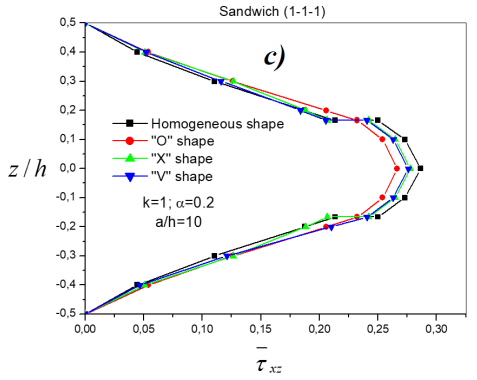

(c) for $k = 1$

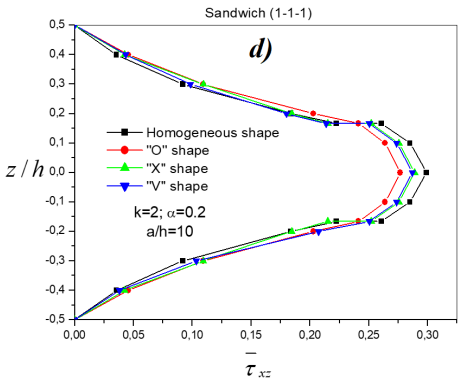

(d) for $k = 2$

Fig. 5 Effect of the shape of porosity distribution on the shear stress $\overline{\tau}_{xz}$ across the thickness of an Al/ZrO_2 FGM square sandwich plate (1-1-1)

The variation of porosity coefficient α on the central deflection is illustrated in Fig. 6. The porosity coefficient has an important effect on the deflections mainly for the homogeneous shape of porosity distribution where the increasing of porosity coefficient increases the central deflections. With increasing of the porosity parameters, the difference among of porosity parameters increases considerably.

4. Conclusions

The presented study is focused on the effect of the distribution shape of porosity on stress distributions and static deflections FGM sandwich plates with different porosity models by using the Navier method. The kinematics of the plate model is based on the higher order shear deformation theory. The properties of the material are assumed to vary according to the thickness direction of the plate and the rule of the mixture that has been reformulated to evaluate the characteristics of the materials with different

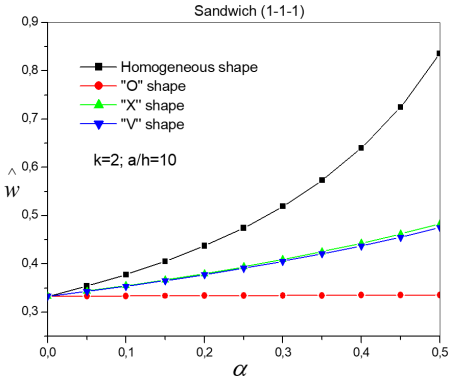

Fig. 6 Effect of porosity coefficient on center deflection FGM sandwich plate (1-1-1) (k = 2)

distribution shape of porosity. A parametric study was conducted, including volume fraction indices, geometry ratios, thickness ratios, volume fraction of porosity and the shape of porosity. According to the typical results, it can be concluded that distribution shape of porosity has a significant effect on the deflections of FGM sandwich plates as well as on the normal and shear stress developed in the sandwich plate. The value of volume fraction and the side-to-thickness ratio are very effective in the porosity effects. With the porosity effects, the stress distribution of the FGM sandwich plates change considerably. In view of this research, it is very important to study the effect of boundary conditions, and to see how these boundary conditions can affect the stability of this type of porous plate.

References

Akavci, S.S. (2010), "Two new hyperbolic shear displacement models for orthotropic laminated composite plates", *Mech. Compos. Mater.*, **46**(2), 215-226. https://doi.org/10.1007/s11029-010-9140-3

Akbaş, Ş.D. (2017), "Vibration and static analysis of functionally graded porous plates", *J. Appl. Computat. Mech.*, **3**(3),199-207. https://doi.org/10.22055/JACM.2017.21540.1107

Al Jahwari, F. and Naguib, H.E. (2016), "Analysis and homogenization of functionally graded viscoelastic porous structures with a higher order plate theory and statistical based model of cellular distribution", *Appl. Mathe. Modell.*, **40**(3), 2190-2205. https://doi.org/10.1016/j.apm.2015.09.038

Avcar, M. (2019), "Free vibration of imperfect sigmoid and power law functionally graded beams", *Steel Compos. Struct., Int. J.*, **30**(6), 603-615. https://doi.org/10.12989/scs.2019.30.6.603

Chen, D., Yang, J. and Kitipornchai, S. (2017), "Nonlinear vibration and postbuckling of functionally graded grapheme reinforced porous nanocomposite beams", *Compos. Sci. Technol.*, **142**, 235-245. https://doi.org/10.1016/j.compscitech.2017.02.008

Ebrahimi, F. and Jafari, A. (2016a), "A higher-order thermomechanical vibration analysis of temperature-dependent FGM beams with porosities", *J. Eng.* http://dx.doi.org/10.1155/2016/9561504

Ebrahimi, F., Ghasemi, F. and Salari, E. (2016b), "Investigating thermal effects on vibration behavior of temperaturedependent compositionally graded Euler beams with porosities", *Meccanica*, **51**(1), 223-249. https://doi.org/10.1007/s11012-015-0208-y

Ebrahimi, F., Dabbagh, A. and Rastgoo, A. (2019), "Vibration analysis of porous metal foam shells rested on an elastic substrate", *J. Strain Anal. Eng. Des.*, **54**(3), 199-208. https://doi.org/10.1177/0309324719852555

Faghidian, S.A. (2014), "A smoothed inverse eigenstrain method for reconstruction of the regularized residual fields", *Int. J. Solids Struct.*, **51**(25-26). https://doi.org/10.1016/j.ijsolstr.2014.09.012

Faghidian, S.A. (2015), "Inverse determination of the regularized residual stress and eigenstrain fields due to surface peening", *J. Strain Anal. Eng. Des.*, **50**(2), 84-91. https://doi.org/10.1177/0309324714558326

Faghdian, S.A. (2020a), "Two phase local/nonlocal gradient mechanics of elastic torsion", *Math. Meth. Appl. Sci.* https://doi.org/10.1002/mma.6877

Faghdian, S.A. (2020b), "Higher order mixture nonlocal gradient theory of wave propagation", *Math. Meth. Appl. Sci.* https://doi.org/10.1002/mma.6885

Faghdian, S.A. (2020c), "Higher–order nonlocal gradient elasticity: A consistent variational theory", *Int. J. Eng. Sci.*, **154**, 103337. https://doi.org/10.1016/j.ijengsci.2020.103337

Farrahi, G.H., Faghidian, S.A. and Smith, D.J. (2009), "An inverse approach to determination of residual stresses induced by shot peening in round bars", *Int. J. Mech. Sci.*, **51**(9-10), 726-731. https://doi.org/10.1016/j.ijmecsci.2009.08.004

Fazzolari, F.A. (2018), "Generalized exponential, polynomial and trigonometric theories for vibration and stability analysis of porous FG sandwich beams resting on elastic foundations", *Compos. Part B: Eng.*, **136**, 254-271. https://doi.org/10.1016/j.compositesb.2017.10.022

Hadji, L. and Avcar, M. (2021), "Free Vibration Analysis of FG Porous Sandwich Plates under Various Boundary Conditions", *J. Appl. Comput. Mech.*, **7**(2), 505-519. https://doi.org/10.22055/JACM.2020.35328.2628

Hadji, L., Zouatnia, N. and Bernard, F. (2019), "An analytical solution for bending and free vibration responses of functionally graded beams with porosities: Effect of the micromechanical models", *Struct. Eng. Mech., Int. J.*, **69**(2), 231-241. https://doi.org/10.12989/sem.2019.69.2.231

Jouneghani, F.Z., Dimitri, R. and Tornabene, F. (2018), "Structural response of porous FG nanobeams under hygro-thermo-mechanical loadings", *Compos. Part B: Eng.*, **152**, 71-78. https://doi.org/10.1016/j.compositesb.2018.06.023

Keddouri, A., Hadji, L. and Tounsi, A. (2019), "Static analysis of functionally graded sandwich plates with porosities", *Adv. Mater. Res., Int. J.*, **8**(3), 155-177. https://doi.org/10.12989/amr.2019.8.3.155

Kitipornchai, S., Chen, D. and Yang, J. (2017), "Free vibration and elastic buckling of functionally graded porous beams reinforced by graphene platelets", *Mater. Des.*, **116**, 656-665. https://doi.org/10.1016/j.matdes.2016.12.061

Merazi, M., Hadji, L., Hassaine Daouadji, T., Tounsi A. and Adda Bedia, E.A. (2015), "A new hyperbolic shear deformation plate theory for static analysis of FGM plate based on neutral surface position", *Geomech. Eng., Int. J.*, **8**(3), 305-321. https://doi.org/10.12989/gae.2015.8.3.305

Nguyen, D.D., Quang, V.D., Nguyen, P.D. and Chien, T.M. (2018), "Nonlinear dynamic response of functionally graded porous plates on elastic foundation subjected to thermal and mechanical loads", *J. Appl. Computat. Mech.*, **4**(4), 245-259. https://doi.org/10.22055/JACM.2018.23219.1151

Ramteke, P.M., Panda, S.K. and Sharma, N. (2019), "Effect of grading pattern and porosity on the eigen characteristics of porous functionally graded structure", *Steel Compos. Struct., Int. J.*, **33**(6), 865-875. https://doi.org/10.12989/scs.2019.33.6.865

Şimşek, M. and Aydın, M. (2017), "Size-dependent forced vibration of an imperfect functionally graded (FG) microplate with porosities subjected to a moving load using the modified couple stress theory", *Compos*. *Struct*., **160**, 408-421. https://doi.org/10.1016/j.compstruct.2016.10.034

Shahsavari, D., Shahsavari, M., Li, L. and Karami, B. (2018), "A novel quasi-3D hyperbolic theory for free vibration of FG plates with porosities resting on Winkler/Pasternak/Kerr foundation", *Aerosp*. *Sci*. *Technol*., **72**, 134-149. https://doi.org/10.1016/j.ast.2017.11.004

Taati, E. and Fallah, F. (2019), "Exact solution for frequency response of sandwich microbeams with functionally graded cores", *J*. *Vib*. *Control*, **25**(19-20), 2641-2655. https://doi.org/10.1177/1077546319864645

Thai, H.T., Nguyen, T.K., Vo, T.P. and Lee, J. (2014), "Analysis of functionally graded sandwich plates using a new first-order shear deformation theory", *Eur*. *J*. *Mech*.*-A*/*Solids*, **45**, 211-225. https://doi.org/10.1016/j.euromechsol.2013.12.008

Wattanasakulpong, N. and Ungbhakorn, V. (2014), "Linear and nonlinear vibration analysis of elastically restrained ends FGM beams with porosities", *Aerosp*. *Sci*. *Technol*., **32**(1), 111-120. https://doi.org/10.1016/j.ast.2013.12.002

Wattanasakulpong, N., Prusty, B.G., Kelly, D.W. and Hoffman, M. (2012), "Free vibration analysis of layered functionally graded beams with experimental validation", *Mater*. *Des*., **36**, 182-190. https://doi.org/10.1016/j.matdes.2011.10.049

Wu, D., Liu, A., Huang, Y., Huang, Y., Pi, Y. and Gao, W. (2018), "Dynamic analysis of functionally graded porous structures through finite element analysis", *Eng*. *Struct*., **165**, 287-301. https://doi.org/10.1016/j.engstruct.2018.03.023

Xu, K., Yuan, Y. and Li, M. (2019), "Buckling behavior of functionally graded porous plates integrated with laminated composite faces sheets", *Steel Compos*. *Struct*., *Int*. *J*., **32**(5), 633-642. https://doi.org/10.12989/scs.2019.32.5.633

Yang, J., Chen, D. and Kitipornchai, S. (2018), "Buckling and free vibration analyses of functionally graded graphene reinforced porous nanocomposite plates based on Chebyshev-Ritz method", *Compos*. *Struct*., **193**, 281-294. https://doi.org/10.1016/j.compstruct.2018.03.090

Zenkour, A.M. (2005), "A comprehensive analysis of functionally graded sandwich plates: Part 1—Deflection and stresses", *Int*. *J*. *Solids Struct*., **42**(18-19), 5224-5242. https://doi.org/10.1016/j.ijsolstr.2005.02.015

Zhao, J., Xie, F., Wang, A., Shuai, C., Tang, J. and Wang, Q. (2019), "Vibration behavior of the functionally graded porous (FGP) doubly-curved panels and shells of revolution by using a semi-analytical method", *Compos*. *Part B*: *Eng*., **157**, 219-238. https://doi.org/10.1016/j.compositesb.2018.08.087

Zhu, J., Lai, Z., Yin, Z., Jeon, J. and Lee, S. (2001), "Fabrication of ZrO2–NiCr functionally graded material by powder metallurgy", *Mater*. *Chem*. *Phys*., **68**, 130-135. https://doi.org/10.1016/j.prostr.2020.06.006